Abiotic Reactivity of De Novo Designed Artificial Copper Peptides (ArCuPs): The Case of C-H Activation

Divyansh Prakash, Suchitra Mitra, Morgan Murphy, Saumen Chakraborty*

Department of Chemistry and Biochemistry, University of Mississippi, University, MS 38677, USA

ABSTRACT: We report a series of de novo designed Artificial Cu Peptides (ArCuPs) that oxidize and peroxygenate C-H bonds of model abiotic substrates via electrochemically generated Cu-oxygen species using H_2O_2 as the terminal oxidant, akin to native Cu enzymes. Detailed assessment of kinetic parameters established the catalytic nature of the ArCuPs. Selective alteration of outer sphere steric at the ***d*** layers above and below the Cu site allows facilitated access of substrates, where a more pronounced effect on catalysis is observed when space is created at the ***d*** layer below the Cu site via Ile to Ala mutation producing a k_{cat} of 6.2 s^{-1}, TON_{max} of 14800 and catalytic proficiency ($k_{cat}/K_M/k_{uncat}$) of 340 M^{-1} for the oxidation of benzyl alcohol. Independent spectroscopic studied revealed that the rate of formation of the Cu-oxygen species and the spectroscopic feature of the most active variant is distinct compared to the other ArCuPs. Systematic alteration of outer sphere hydrophobicity led to a correlated tuning of the T2 Cu site redox potentials by ~80 mV. The enhanced activity of the ArCuP variant is attributed to a combination of steric effect that allows easy access of substrates, the nature of Cu-oxygen species, and stability of this construct compared to others, where Ile to Ala mutation unexpectedly leads to a higher thermostability which is further augmented by Cu binding.

INTRODUCTION

Copper (Cu) containing proteins carry out diverse functions in biology starting from electron transfer (ET) to substrate activation, thanks to the abundance of Cu in the geosphere, its accessible redox potentials ($E^{0'}$), and favorable electronic properties.[1] The protein scaffold controls the coordination number, ligand environment, and geometry, which further fine-tunes the physical and reactivity properties of Cu. While the type I (T1) Cu proteins are exclusively involved in ET, the T2 Cu proteins participate in both ET and substrate activation. For example, in non-coupled binuclear enzyme peptidyl glycine α-hydroxylating monooxygenase (PHM), the substrate activation occurs at a T2 Cu_M center featuring $Cu(His)_2Met$ coordination, while the second T2 Cu_H site ~11Å away with a $Cu(His)_3$ coordination participates in ET (Fig. 1A). PHM catalyzes the activation of C-H bonds (BDE ~89 kcal/mol), in some cases showing regioselectivity for secondary C-H bonds over primary C-H bonds.[1c] Galactose oxidase (GO) is a monocopper enzyme that oxidizes primary alcohols to aldehydes using molecular O_2. Lytic polysaccharide monooxygenases (LPMOs) are mononuclear T2 Cu enzymes (Fig. 1B) that degrade recalcitrant polysaccharides into simpler precursors for biofuels and other useful products.[2] Discovery of LPMOs are attractive from both fundamental science and industrial perspectives to degrade cellulosic biomass into useful chemicals using both O_2 and H_2O_2 as terminal oxidants. The reaction rates are greatly accelerated when H_2O_2 is used instead of O_2 under reducing conditions, leading to the implication that these enzymes are peroxygenases instead of monooxygenases.[3] In addition to the active site, the local environment and outer coordination sphere interactions play crucial roles in tweaking the activity of Cu enzymes.[1c] For example, hemocyanin (Hc) and tyrosinase (Ty) are structurally similar, both have binuclear Cu---Cu active sites and produce similar $Cu\text{-}O_2$ intermediates. Yet, Ty shows mono and di-phenolase activity, while Hc does not. This differential reactivity has been attributed to differences in substrate access between these two proteins.[1c, 4] From enzymatic and modeling studies superoxo ($Cu^{II}\text{-}O_2^{\bullet-}$), hydroperoxo ($Cu^{II}$-OOH), and high-valent oxo (Cu≡O) or oxyl ($Cu^{II}\text{-}O_2^{\bullet}$) type intermediates have been proposed to form as the reactive species in Cu enzymes.[1c, 5]

Design of artificial metalloenzymes (ArMs) as functional analogues of native enzymes is an attractive approach for the development of efficient and sustainable biocatalysts.[6] We have been employing de novo protein design approach to create artificial Cu proteins (ArCuPs) within self-assembling scaffolds.[7] A particular focus is to expand the functional diversity of these constructs into previously unexplored areas,[8] including energy relevant catalysis.[7, 9] As complex enzyme structures are made up of peptides, which are subsequently synthesized from amino acid building blocks, de novo metalloenzyme design approach provides a handle to explore how primary sequence determines the folding and function of complex metalloenzymes.[10] In addition, the simpler de novo proteins help elucidate the catalytic and mechanistic underpinning of complex native enzymes. Pre-defined rules to create specific oligomeric assemblies of de novo design[11] allows an unprecedented control over the

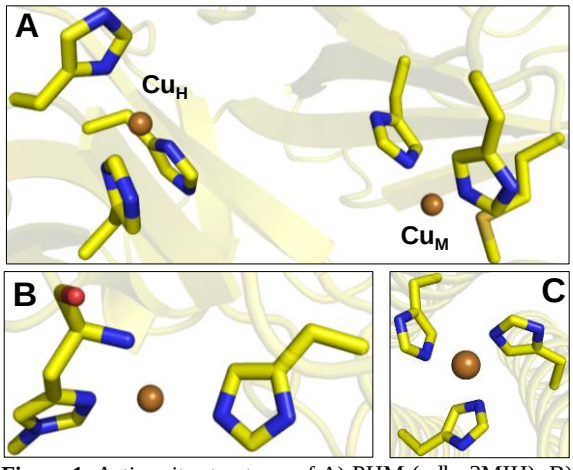

Figure 1. Active site structures of A) PHM (pdb: 3MIH), B) LPMO (pdb: 2YET), and C) 3SCC (pdb: 7L33).

coordination number, protein stability, and non-covalent interactions to fine tune the physical and catalytic properties of these ArMs.

We have recently reported the design, structural characterization and H_2O_2 activation properties by a trimeric ArCuP (3SCC) featuring a $Cu(His)_3$ active site (Fig. 1C).[7] Herein, we expand the repertoire of reactivity of 3SCC into activation of C-H bonds of model substrates with varying CH_{BDE} using Cu-oxygen species generated with H_2O_2 under reducing conditions as reactive intermediates. Outer sphere steric are systematically altered to control substrate access, influence the rates of Cu-oxygen species formation, tune the $E^{0'}$s, and to alter the stability of the ArCuPs. We find that local packing effects dictate how removal of steric bulk in one side of the Cu site preferentially enhances catalysis (k_{cat}) and favors substrate binding (K_M), ultimately tuning the catalytic proficiency (k_{cat}/K_M)/k_{uncat}. A delicate relationship between substrate accessibility, rates, E^0s, and peptide stability is found, which ultimately control the reactivity pattern.

RESULTS AND DISCUSSION

1. Catalysis

i. Electrocatalysis: The catalytic properties of ArCuPs were studied using protein film voltammetry (PFV) using H_2O_2 as the terminal oxidant. Analogous to heme systems employing O_2,[12] the premise is centered on the hypothesis that the electrochemically generated reactive Cu-oxygen intermediates are potent oxidants to activate C-H bonds. Substrates **1**-**5** with varying C-H_{BDE} of 85-98 kcal/mol are chosen (Scheme 1) in this study. The catalytic response of 3SCC adsorbed as films (0.125 mM) on PGE is assessed by following linear sweep voltammograms (LSVs) with substrates in the presence of 100-fold H_2O_2. Previously we have shown that the saturating concentration for H_2O_2 is ~12.5 mM,[7] which is why all experiments are performed with 12.5 mM H_2O_2. In the absence of substrates, reduction of H_2O_2 occurs (Fig. 2A dark yellow).[7] In the presence of substrates **1**-**5** (**1**-black; **2**-blue; **3**-red; **4**-olive; **5**-orange), large catalytic currents with onset potentials (E_{onset}) of ~50 mV vs Ag/AgCl are observed (Fig. 2A). The blank electrode does not show any appreciable current with H_2O_2 (gray), in presence of substrate (**1**-violet), and in the presence of both H_2O_2 and **1** (dark gray). Further control experiments with 3SCC and the substrate, but in the absence of H_2O_2 did not show catalytic response (navy). This result suggests that H_2O_2 is necessary as the terminal oxidant and that the Cu-oxygen intermediate is the active species, which is why catalytic currents of ArCuPs are observed only in the presence of both H_2O_2 and substrate(s). In the absence of H_2O_2, the Cu-OOH intermediate is not formed and therefore no catalytic response is observed. To establish that the observed

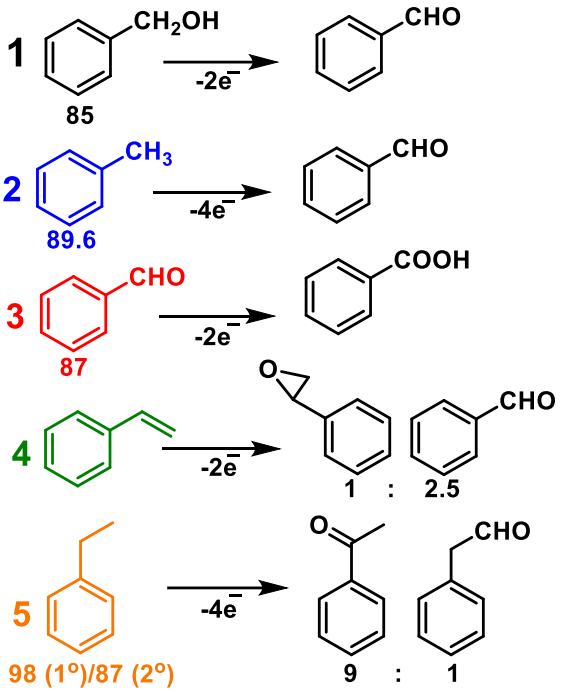

Scheme 1. Substrates used in this study and the corresponding products formed.

activity is attributable to the $Cu(His)_3$ active site and not from adventitiously bound Cu, the active site His residues were replaced with Ile. The 3SCC-His variant (Table 1 shows the sequence), owing to its inability to bind Cu and therefore the lack of formation of the reactive species, showed negligible current as compared to 3SCC (Fig. 2A wine) in the presence of H_2O_2 and **1**. This result highlights the importance of the active site to enable catalysis.

ii. Product analysis: In order to detect and quantify the products of electrochemical oxidation, controlled potential electrolysis (CPE) experiments were performed at -950 mV vs Ag/AgCl for 1h to generate the oxidation products. At the end of electrolysis, the products were extracted in dichloromethane and detected using gas chromatography (GC). These analyses led to the identification of the products as benzaldehyde from **1** and **2**, benzoic acid from **3**, styrene oxide and benzaldehyde (in 1:2.5 ratio) from **4.** The amount of charge passed during electrolysis (Fig. 2B, Fig. S1-5) was significantly large, ~6-fold, with 3SCC/H_2O_2/substrates compared to the control experiments with 3SCC-His/H_2O_2/substrates. No product was observed for either the blank electrode (without 3SCC) or with 3SCC-His/H_2O_2/substrates. To probe regioselectivity, ethylbenzene **5** was employed.

Table 1. Peptides and their sequences used in this study.

Peptide	Sequence
3SCC	Ac GIAAIKQE HAAIKQE IAAIKQE IAAIKWEG $CONH_2$
3SCC-His	Ac GIAAIKQE IAAIKQE IAAIKQE IAAIKWEG $CONH_2$
I5A-3SCC	Ac GIAAAKQE HAAIKQE IAAIKQE IAAIKWEG $CONH_2$
I12A-3SCC	Ac GIAAIKQE HAAAKQE IAAIKQE IAAIKWEG $CONH_2$
I5AI12A-3SCC	Ac GIAAAKQE HAAAKQE IAAIKQE IAAIKWEG $CONH_2$

The oxidation products of **5** are acetophenone (2° C-H bond) and phenylacetaldehyde (1° C-H bond) produced at a ratio of 9:1. This result suggests that the Cu-oxygen species selectively oxidizes benzylic C-H bonds (C-H_{BDE} = 85 kcal/mol) of **5** over primary C-H bonds (C-H_{BDE} = 98 kcal/mol), similar to what is observed in PHM as well.[1c] Together, these results demonstrate that the 3SCC ArCuP supports multi-electron oxidation and peroxygenation processes, and that the designed $Cu(His)_3$ site is where the substrate activation occurs.

iii. Assessment of catalytic activity: The catalytic efficiency (k_{cat}/K_M) is determined in the pH range of 5.5-9.5 (Fig. S6-7), which shows that the maximum activity occurs at pH 6.5 (Fig. 2C). The relevant catalytic parameters are shown in Table 2. The highest k_{cat} of ~3.5 s^{-1} and turnover number (TON) of ~$8.2x10^3$ for 3SCC was obtained with **1** and **4**. The K_M was in mM range for all the substrates, with the lowest K_M of 22.7 mM for **5**. The highest catalytic proficiency I/K_{TS} (k_{cat}/K_M)/k_{uncat} (K_{TS} is the apparent transition-state binding affinity;[13] k_{uncat} is obtained with 3SCC-His variant) was observed for **1**. To obtain mechanistic insight and to determine the rate determining step (RDS), a Hammett analysis was performed. The activity of *p*-substituted derivatives of **1** varied with electron withdrawing substituents (-OMe, -Me, -Cl, -NO_2) producing a linear correlation with a negative slope (ρ) of -0.5 (Fig. 2D), suggesting that a positive charge is created in the rate-determining step (RDS). A similar ρ value has been observed in GO[14] and a synthetic complex[5h] reported by Itoh and coworkers. A primary kinetic isotope effect (KIE = k_H/k_D) of 2.8 was obtained for $PhCD_2OH$, which indicate that H-atom transfer (HAT) is the RDS.

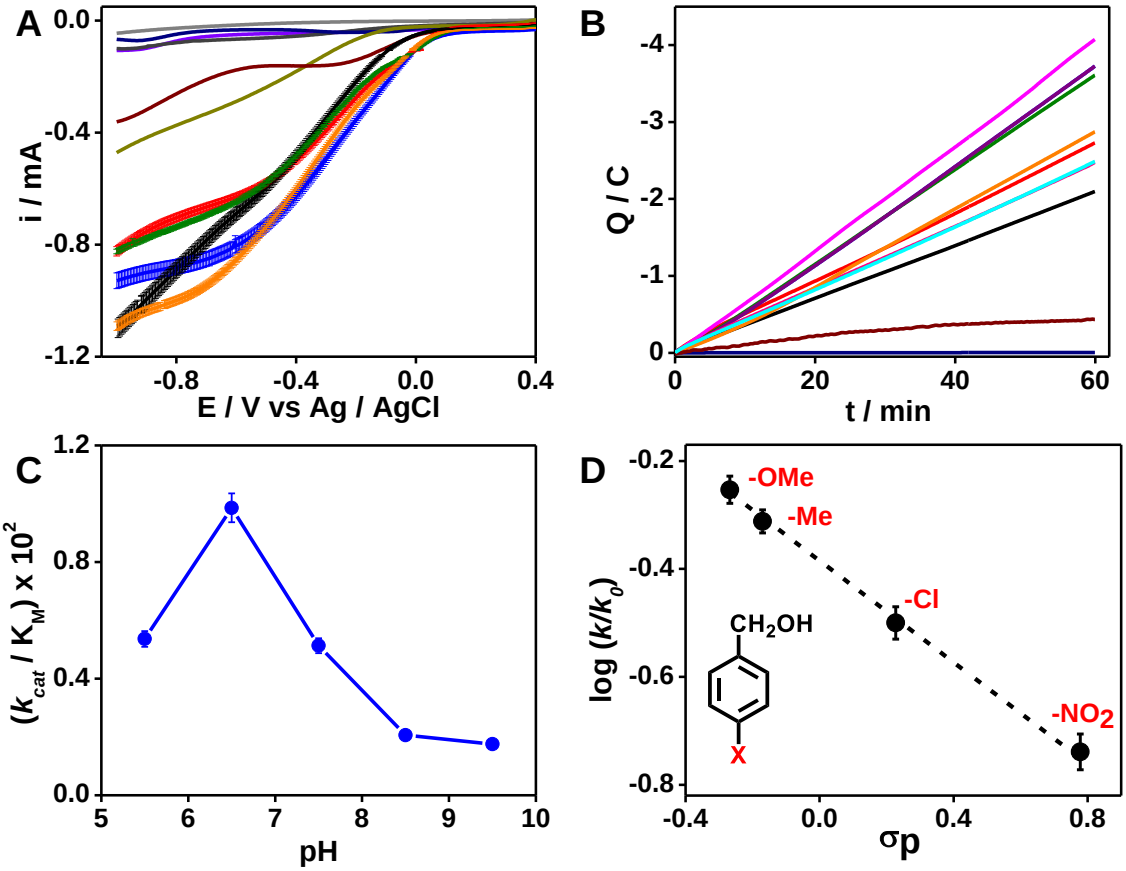

Figure 2. A) LSVs of blank SWNT/PBSE on GCE in the presence of H_2O_2 (gray); in the presence of **1** but without H_2O_2 (violet); in the presence of both H_2O_2 and **1** (dark gray). The corresponding LSVs for 3SCC + **1** (navy); 3SCC + H_2O_2 (dark yellow; H_2O_2 reduction); 3SCC + H_2O_2 + **1-5**: (**1** = black, **2** = red, **3** = blue, **4** = olive, **5** = orange); 3SCC-His + H_2O_2 + **1** (wine). In all the experiments, [3SCC] = 0.125 mM, [H_2O_2] = 12.5 mM, and [**1-5**] = 125 mM. 10 μL of SWNT/PBSE/peptide samples were dropped on GCE and the film was dried under a gentle flow of N_2. The LSVs were recorded in N_2 saturated 80 mM mixed buffer at pH 6.5 with v = 100 mVs^{-1}. The shaded region represents error bars from three separate experiments of fresh protein films at each condition. B) Q vs t traces from 1h CPE experiments performed at -950 mV vs Ag/AgCl. Blank electrode SWNT/PBSE + H_2O_2 + **1** (navy); 3SCC + H_2O_2 + **1** (black); I5A-3SCC + H_2O_2 + **1** (red); I12A-3SCC + H_2O_2 + **1** (blue); and I5AI12A-3SCC + H_2O_2 + **1** (olive). Traces are also shown for I12A-3SCC + H_2O_2 + **1-5** where **1** = purple, **2** = cyan, **3** = magenta, **4** = pink, and **5** = orange; and the control peptide 3SCC-His + H_2O_2 + **1** (purple). C) Plot of k_{cat} / K_M vs pH for the electrocatalytic oxidation of **1** to benzaldehyde. D) Hammett analysis of p-substituted derivatives of **1** in presence of H_2O_2 and 3SCC. All experiments were performed in N_2-saturated buffers.

Table 2. Catalytic parameters of the ArCuPs for **1-5** at pH 6.5 extracted from data in Fig. 2, Fig. S1-7.

ArCuP	Parameters	1	2	3	4	5
3SCC	k_{cat} / s^{-1}	3.5	2.3	2.3	3.4	1.5
	K_M / mM	35.7	23.3	27.9	42.1	19.8
	$1/k_{TS}$ x10^2 /M^{-1}	1.9	1.4	1.2	0.6	0. 8
	TON_{max} x 10^3	8.2	5.8	5.6	8.1	5.5
15A-3SCC	k_{cat} / s^{-1}	4.5	2.7	2.4	3.7	1.9
	K_M / mM	32.3	25.8	27.1	40.8	22.7
	$1/k_{TS}$ x10^2 /M^{-1}	2.6	1.5	1.3	0.7	0.9
	TON_{max} x 10^3	10.7	6.6	5.9	9	6.9
I12A-3SCC	k_{cat} / s^{-1}	6.2	3.3	4.1	4.1	2.4
	K_M / mM	34.7	20	18.4	31.8	24
	$1/k_{TS}$ x10^2 /M^{-1}	3.4	2.4	3.3	1.1	1.1
	TON_{max} x 10^3	14.8	7.9	9.9	9.9	8.6
I5AI12A-3SCC	k_{cat} / s^{-1}	6	3	4	3.6	2.1
	K_M / mM	39.7	36	40.8	66.6	26.9
	$1/k_{TS}$ x10^2 /M^{-1}	2.9	1.2	1.4	0.4	0.9
	TON_{max} x 10^3	14.3	7.4	9.6	8.7	7.8

2. Selective alteration of outer sphere steric enhances the rates, reactivity, and $E^{0'}$

i. Design considerations: Inspection of the 3SCC structure reveals that bulky hydrophobic residues pack above (Fig. 3A) and below (Fig. 3B) the Cu site, which can restrict substrate access. To probe how altering outer sphere sterics around Cu changes the physical and catalytic properties of the ArCuPs, Ile residues at both the ***d*** sites above and below the $Cu(His)_3$ site are replaced with Ala. The smaller -CH_3 side chain of Ala is expected to provide a more facile access of substrates into the active site and change the polarity of the peptide interior. Gly was not chosen due to its flexibility which can break 2° structures. Ala on the contrary, is a helix inducer. PyMol models of Ala mutants based on the x-ray structure of 3SCC indeed show that space is created in both I5A-3SCC (Fig. 3C) and I12A-3SCC (Fig. 3D) mutants. It is also intriguing that more space is created towards the C-termini, i.e. via the I12A mutation than the corresponding N-termini side, as internal packing is controlled according to the helical twist within the core. The double mutant I5AI12A-3SCC is also prepared and tested.

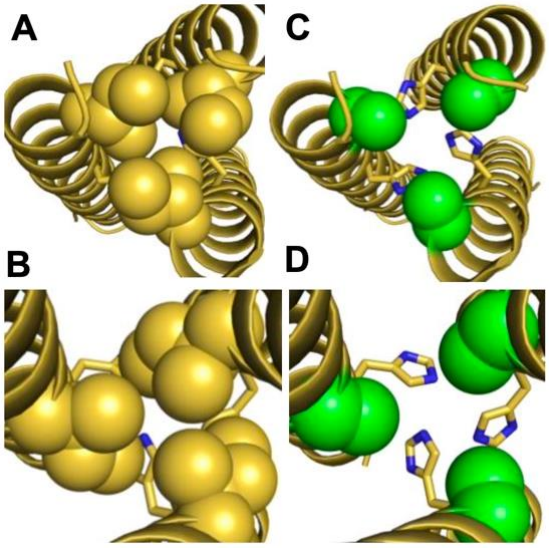

Figure 3. Packing of the *d* site Ile (yellow spheres) immediately above (A) and below (B) the His site of Cu-3SCC. Ile to Ala (green spheres) substitution of the corresponding sites to opens up space at the outer sphere (C, D).

ii. Rates of Cu-oxygen species formation: The formation of Cu-oxygen species was monitored by UV-vis under anaerobic conditions. Previously, we that shown that Cu^{II}-3SCC reacts with H_2O_2 to form Cu-hydroperoxo species with a rate of 1.4 x 10^{-6} s^{-1}, which was accelerated by ~100-fold in Cu^{I}-3SCC.[7] We have also shown that the differences in the spectral features with oxidized vs reduced forms of the peptide and H_2O_2 is attributed to differences in the His oxidation, which was observed with Cu^{I}-3SCC and not with Cu^{II}-3SCC. With both Cu^{II} and Cu^{I} forms of the variants, slight differences in λ_{max} of the Cu-OOH species are present (Fig. 4) compared to that of 3SCC (Table 3), indicating differences in the electronic environment around the active site. In Cu^{II}-form, the I5A-3SCC and I5AI12A-3SCC have a similar λ_{max} of 365 nm (Fig. 4 A,C) and rates of 8.9-6.4 x 10^{-6} s^{-1} (Table 3; Fig. S8).

Table 3. Parameters from UV-vis kinetics.

Sample	ε ($M^{-1}cm^{-1}$) (λ_{max})	Initial rate (s^{-1})	ε ($M^{-1}cm^{-1}$) (λ_{max})	Initial rate (s^{-1})
I5A-3SCC	4.3 x 10^2 (365)	8.9 x 10^{-6}	1.8 x 10^3 (346)	4.6 x 10^{-4}
I12A-3SCC	1.3 x 10^2 (374)	3.0 x 10^{-5}	1.9 x 10^3 (335)	4.7 x 10^{-4}
I5AI12A-3SCC	2.4 x 10^2 (365)	6.4 x 10^{-6}	2.1 x 10^3 (346)	4.0 x 10^{-4}

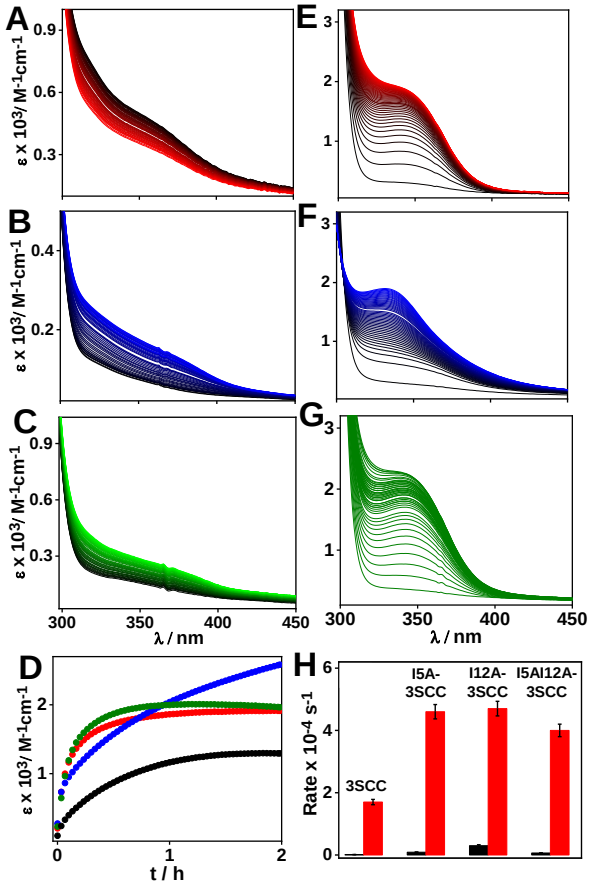

Figure 4. UV-vis kinetics of H_2O_2 reaction with Cu^{II}/Cu^{I} bound peptides I5A-3SCC (A/E), I12A-3SCC (B/F), and I5AI12A-3SCC (C/G). Shown are the time dependent spectra after addition of 12.5 mM H_2O_2 to 0.125 mM peptides in N_2-saturated 10 mM MES buffer at pH 6.5. (D) Time traces of the Cu^{I}-ArCuPs at respective λ_{max} (black = 3SCC, red = I5A-3SCC, blue = I12A-3SCC, olive = I5AI12A-3SCC). E) Initial rates of formation of Cu-OOH species in the Cu^{II} (black) and Cu^{I} forms (red).

In contrast, the Cu-OOH species in I12A-3SCC has a λ_{max} of 374 nm (Fig. 4B) and rate of 3 x 10^{-5} s^{-1}, which is approximately an order of magnitude higher than the other variants and the parent 3SCC. In the Cu^{I}-form, the peaks blue shifted to 346 nm for I5A-3SCC (Fig. 4E) and I5AI12A-3SCC (Fig. 4G), and to 335 nm for I12A-3SCC (Fig. 4F). The rates of formation of Cu-OOH species are accelerated to ~10^{-4} s^{-1} with Cu^{I}-forms (Fig. 4 D, H; Table 3). The higher rates with Cu^{I}-peptides are owing to the more reactive nature of Cu^{I}/H_2O_2 than Cu^{II}/H_2O_2, a conclusion which is consistent with what is observed in LPMO as well.[3, 5b, 15] The rate enhancement in the variants compared to the parent 3SCC is indicative of a facilitated access of H_2O_2 to the Cu site of the variants. These data also hint reactivity differences in the mutants, where the I12A-3SCC variant clearly displaying differences in the nature of Cu-oxygen species and the rate of its formation compared to the other two variants, which reflect the differences in substrate oxidation ability of this variant compared to others (*vide infra)*.

iii. Differences in oxidative reactivity: Among all the ArCuPs investigated here, the highest k_{cat} and TON was obtained with I12A-3SCC for all the substrates (Fig. S9, Table 2), while the WT 3SCC had the lowest k_{cat}. In general, K_M is lower in I12A-3SCC among the ArCuPs. Substrates **2** and **5** have lower K_M than others. The catalytic proficiency is the highest for I12A-3SCC irrespective of the substrate (Fig. 5, Table 2). Another obvious trend is that the I5A-3SCC and I5AI12A-3SCC have comparable catalytic proficiency. This observation is intriguing, since we expected that opening up space both above and below the Cu site in I5AI12A-3SCC would allow better access of substrates than either I15A-3SCC or I12A-3SCC.

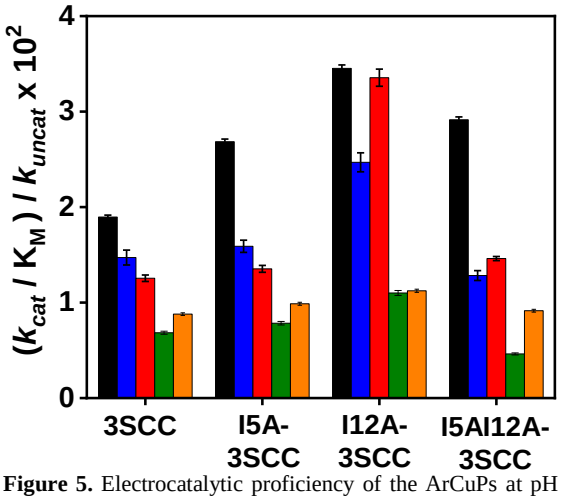

Figure 5. Electrocatalytic proficiency of the ArCuPs at pH 6.5. k_{cat} and k_{uncat} were obtained from the catalyzed and uncatalyzed reactions with the ArCuPs and the 3SCC-His mutant, respectively. K_M is obtained from data in Fig. S1-5 at different concentrations of substrates. **1** (black), **2** (blue), **3** (red), **4** (olive), and **5** (orange).

However, this is not observed. This trend is consistent nonetheless, with the fact that similar spectral features and rates of formation of the Cu-oxygen species in I5A-3SCC and I5AI12A-3SCC (Fig. 4, Table 3). The favorable reactivity for the I12A-3SCC mutant is likely attributable to the more space created below the Cu site allowing preferential access of H_2O_2 and substrates.

iv. Modulating outer sphere hydrophobicity tunes $E^{0'}$: We investigated how changes in the hydrophobicity due to outer sphere mutations alters the redox properties of the ArCuPs. Cyclic voltammograms for all the variants indicate the quasi-reversible nature of the redox process from well-defined protein films on the electrode (Fig. 6). The highest redox reversibility is observed for I5AI12A-3SCC (Fig. 6 olive) with a ΔE_p = 4 mV (Table 4) followed by I12A-3SCC (Fig. 6 blue). The I5A-3SCC (Fig. 6 red) with a ΔE_p of 80 mV is the least reversible system. Both the cathodic and anodic peaks have large full width at half height ($\Delta E_{1/2c}$, $\Delta E_{1/2a}$) which deviates from the theoretical value of 91mV for an ideal and reversible $1e^-$ redox process, suggesting that dispersion and electrostatic effects influence the redox process.[16] The peak currents show a linear dependence with scan rate, indicating a surface controlled redox process (Fig. S10). The positive $E^{0'}$ for all the mutants signify that the reduced forms of ArCuPs are more stable than the oxidized forms. The highest $E^{0'}$ is observed for the parent 3SCC peptide (0.256 V) followed by I5A-

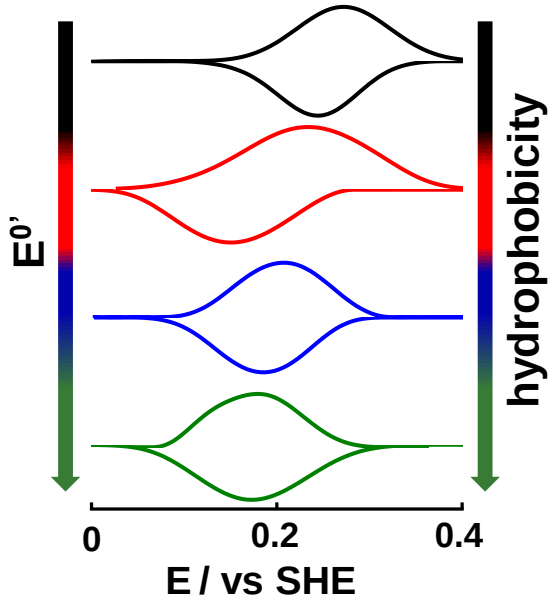

Figure 6. CVs of 3SCC (black), I5A-3SCC (red), I12A-3SCC (blue), and I5AI12A-3SCC (olive) at 50 mVs^{-1} in N_2 saturated 80 mM mixed buffer at pH 6.5. The peptide samples were dropped on PGE and dried under N_2 prior to data collection.

3SCC/I12A-3SCC (0.192 V and 0.198 V). The double mutant I5AI12A-3SCC has the lowest $E^{0'}$ of 0.178 V. With a decrease in hydrophobicity around the active site, the $E^{0'}$s shifted cathodically, implying that as the polarity around Cu is increased, Cu^{II} state becomes more stable than Cu^{I}. In T1 ET protein azurin, modification of hydrophobicity and H-bonding network around Cu ligands have led to the tuning of $E^{0'}$ by ~700 mV.[17] Unlike the T1 Cu proteins that span a wide potential range, the $E^{0'}$ of T2 Cu sites is regulated in a narrow window.[1a, 18] In this context, tuning $E^{0'}$ of the T2 site of the ArCuPs by ~80 mV via modulating outer sphere steric is noteworthy.

Table 4. Redox properties of the ArCuPs at pH 6.5.

Sample	E_{pc} / mV	E_{pa} / mV	$E^{0'}$ / mV	▲E_p /mV	▲$E_{1/2c}$ / mV	▲$E_{1/2a}$ / mV	I_c / µA	I_a / µA
3SCC	239(±6)	273(±5)	256	34	92	132	-7.1 (±0.1)	6.2 (±0.1)
I5A-3SCC	152(±4)	232(±3)	192	80	130	153	-5.9 (±0.1)	5.5 (±0.1)
I12A-3SCC	188(±4)	208(±4)	198	20	106	121	-7.0 (±0.2)	6.3 (±0.1)
I5AI12A-3SCC	176 (±1)	180(±2)	178	4	140	173	-7.1 (±0.1)	7.1 (±0.1)

Although WT 3SCC has the highest $E^{0'}$, a lack of space around Cu limits substrate access and thus its reactivity. When comparing the variants, I5A-3SCC and I12A-3SCC have similar $E^{0'}$, higher than the double mutant. Yet, the catalytic proficiency of I5AI12A-3SCC is comparable to I5A-3SCC. However, despite having a similar $E^{0'}$s, the higher catalytic proficiency of I12A-3SCC than I5A-3SCC cannot be explained solely based on $E^{0'}$.

3. I12A-3SCC is the most stable construct: Unexpected trend. To probe how removal of Van der Waals interactions alters the folding and stability of the ArCuPs, CD spectroscopy was used (Fig. S11). In general, all the variants show characteristics of α-helix in the apo form except I5A12A, which is only weakly helical. In the Cu-bound form, all constructs become more helical. Both apo (Fig. S12) and Cu-3SCC undergo a transition from folded to unfolded state with a t_m of ~65 °C (Fig. 7 black, Table S1). Altering the ***d*** site above the His resulted in decreased stability of I5A-3SCC (Fig. S12) by 12 °C in the apo form compared to the parent construct. This is not unexpected, as Ile to Ala mutation lowers the packing interactions. Here, Cu^{II}-binding has negligible effect in thermostability (Fig. 7 red). Surprisingly, mutation at the ***d*** site

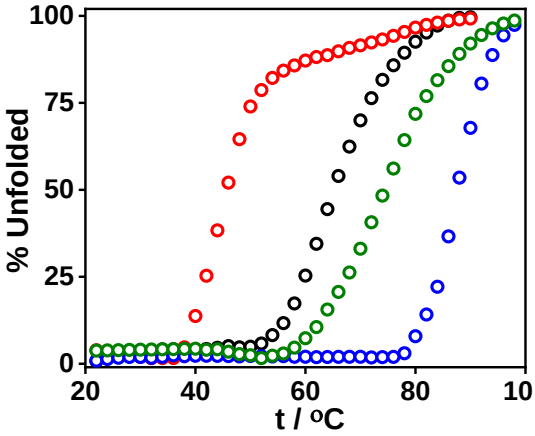

Figure 7. Thermal melting profiles of the ArCuPs (black = 3SCC, red = I5A-3SCC, red = I12A-3SCC, olive = I5AI12A-3SCC) in their Cu^{II}-bound forms monitored at 222 nm. All experiments were performed with 10 µM trimers in 3 mM phosphate buffer at pH 6.5.

below the His led to an increased stability of I12A-3SCC mutant with t_m increasing by 5 °C in the apo form and by 22 °C for the Cu bound peptide (Fig. 7 blue) compares to the 3SCC construct. The thermal melt for apo I5AI12A mutant does not show any obvious folding-unfolding transition (Fig. S12), which is consistent with the CD profile. Cu^{II}-I5AI12A-3SCC behaves well folded and is quite stable with t_m ~ 76 °C (Fig. 7 green). The highest t_m of I12A-3SCC is unexpected as lost Van der Waals packing by Ile to Ala mutation should destabilize the construct relative to the parent 3SCC peptide. It appears that while the Ile/Ile repeat at ***a/d*** site is necessary to produce the trimers, the knob-into-holes packing[19] of Ile residues at the ***d*** site does not produce the most stable assembly. Rather there is a trade-off between producing a specific oligomeric state vs peptide stability. Ile to Ala replacement likely relieves the unfavorable packing effect of ***d*** layer Ile residues. Cu binding further stabilizes the I12A-3SCC leading to a ~19 °C increase in t_m than the apo peptide.

SUMMARY AND CONCLUSIONS

In this work, we have demonstrated the oxidation and peroxygenation as novel functional repertoire supported by de novo designed metalloproteins in regards to activation of C-H bonds. The application of protein electrocatalysis is unprecedented in assessing the functional characteristics of ArMs. The outer sphere interactions of the ArCuPs were systematically modulated by opening space above and below the Cu(His)$_3$ site that improved the rates of Cu-oxygen species formation with H_2O_2 by providing a facile access of the oxidant. A larger space is selectively created towards the C-termini, below the active site than the N-termini, governed by the local packing effects controlled by the helical twist. The reactive intermediates, electrochemically generated cathodic to the redox peak of Cu^{II}-peptides abstract H atom from C-H bonds of substrates. Under reducing conditions, the formation of Cu-OOH species is significantly enhanced. This resonates with LPMO, in that the reductive priming is a critical step in generating reactive species that subsequently facilitates catalysis. A systematic decrease in hydrophobicity introduced by Ile to Ala mutations led to a cathodic shift of $E^{0'}$ as the increased polarity around the Cu site (water access) stabilizes the Cu^{II} state over Cu^{I}. Here, altering the hydrophobicity ~6 Å away from the T2 Cu site tunes the $E^{0'}$ by ~80 mV. Despite having highest $E^{0'}$, I9H-Cu has the lowest activity and is due to the presence of large hydrophobic Ile residues above and below the active site, which hinders substrate access.

We expected I5AI12A-3SCC to be the most active variant as it would allow the most face access of substrates. Surprisingly, the activity of this mutant is less than I12A-3SCC, but comparable to I5A-3SCC. This has bearing to the fact the spectroscopic signatures and the rates of formation of Cu-oxygen species in I5A-3SCC and I5AI12A-3SCC are comparable, implying that similar intermediates are generated in these two variants. In contrast, the spectroscopic features and the rate of formation of the Cu-oxygen species is faster in I12A-3SCC even in the Cu^{II}-form, suggesting that this mutant is inherently more reactive. While the rates become comparable in all variants in the Cu^{I}-form, the spectroscopic features of I5A-3SCC and I15AI12A-3SCC remain similar to each other but distinct from I12A-3SCC. The thermal stability studies show that the I12A-3SCC is the most thermostable among all the studied peptides. This is unexpected as the mutation of Ile to Ala is expected to lower Van der Waals packing and thus destabilize the structure. We attribute to higher catalytic proficiency of I12A-3SCC to the highest stability of this variant along with the unique nature of Cu-oxygen species generated in this variant. The I5A-3SCC is the least stable but the activity is comparable to I5AI12A-3SCC. While I5AI12A-3SCC has a higher stability than I5A-3SCC, the $E^{0'}$ of the former is lower than the latter. Clearly, when assessing the activity trends of the ArCuPs, one must be cognizant about a combined view of stability, $E^{0'}$, and the nature/rates of Cu-OOH intermediates, in addition to substrate accessibility.

A current limitation is the high K_M for the substrates tested. One approach to lower K_M and thus increase catalytic proficiency is to introduce aromatic residues near the Cu site which should allow docking of aromatic substrates by π-π stacking- an approach which will be explored in the future. Indeed, this strategy has been applied in dimeric LmrR based ArMs.[20] A second limitation is that the self-assembling nature of ArCuPs which precludes tuning the reactivity by selective introduction of acidic or basic residues near the Cu site. An Asp residue in the outer sphere has been shown to be a critical factor in the activity of LMPOs.[3b] This aspect will be addressed in future studies via single-chain ArCuP design. In any case, the prospects of this study can be used in de novo design of ArMs and pave the way for developing efficient catalysts for small molecule activation.

EXPERIMENTAL SECTION

Materials and methods. All chemicals and reagents were of analytical grade and used without further purification. All the glassware and plasticware were immersed in a 10 mM ethylenediaminetetraacetic acid bath overnight, followed by soaking in 10% and 1% nitric acid baths, respectively. All buffer solutions were prepared in Milli-Q (Millipore) water and treated with Chelex 100 overnight to remove trace metals. Tris(hydroxymethyl) aminomethane (TRIS), 4-(2-hydroxyethyl)-1-piperazineethanesulfonic acid (HEPES), 3-morpholinopropane-1-sulfonic acid (MOPS), 2-(N-morpholino) ethanesulfonic acid (MES), sodium acetate, NaCl and HCl were purchased from Fisher Scientific. The mixed buffers contained 20 mM each of MES, sodium acetate, HEPES and TRIS. For electrochemistry experiments 0.1 M KCl was added as supporting electrolyte to the mixed buffers. $CuCl_2$ (Alfa Aesar), ascorbic acid (VWR), NaOH (VWR), and H_2O_2 (VWR) stock solutions were made in water. $PhCD_2OH$ used for isotope labeling experiment was purchased from Sigma-Aldrich.

Peptide synthesis and purification. Peptides were synthesized, purified to homogeneity, and their identities verified according to known procedures.[10]

UV-vis Spectroscopy. The UV−vis spectra were recorded on an Agilent 8454 or Cary 5000 spectrophotometer. All samples were prepared in 10 mM MES buffer at pH 6.5. The kinetics experiments were performed with 0.125 mM Cu-peptides after the addition of 12.5 mM H_2O_2 and the kinetics was monitored for 100 min with 60 s interval between scans. For reactions with the Cu(I) form, 125 mM Asc was used before H_2O_2 addition. All components were degassed, and the kinetics was monitored anaerobically in a septa-capped cuvette (Starna Cells). The initial rates were calculated from the first 3 minutes of the kinetic run in each case.

Circular dichroism (CD) spectroscopy. The CD spectra were recorded using a JASCO J-1500 spectrometer. 10 μM trimer peptide samples were prepared in 3 mM Phosphate buffer pH 6.5. Thermal unfolding experiments were performed by monitoring the CD signal at 222 nm in the temperature range of 20–100 °C.

Electrochemistry.

i. Non-catalytic voltammetry: Non-catalytic CV experiments were performed using a Wave Driver 20 bio-potentiostat (Pine Instruments) with pyrolytic graphite electrode (PGE) as the working electrode, coiled platinum wire as the counter electrode, and Ag/AgCl (in saturated KCl) as the reference electrode. 10 μL of 125 μM ArCuPs were drop-cast on PGE followed by 6 μL of 0.1 M polymyxin B to facilitate

electrostatic interaction with the electrode. The drop was dried under N_2, and voltammograms were recorded in N_2-saturated 80 mM mixed buffer solutions with 100 mM KCl as a supporting electrolyte. The potential values were referenced against Ag/AgCl and converted to SHE.

ii. Electrode preparation for catalytic assays: All electrocatalytic experiments were performed using composites on glassy carbon electrode according to literature procedure.[21] Briefly, 0.2% SWNT was dispersed in 4:1 ratio of water: ethanol mixture followed by addition of 0.1% (~17µL) nafion/ethanol. The mixture was then sonicated for 1h at 37º C. To the suspension, aliquots of the hetero bifunctional pyrene linker, 1-pyrenebutyric acid N-hydroxy succinimide ester (4µL of 4mg/mL) (PBSE) dissolved in DMF were added and the mixture was incubated for 1h at RT. The final samples were prepared by mixing SWNT/PBSE composite and the ArCuP in 1:1 ratio and incubated for 12-16 h at 4º C. On one end PBSE linker attaches to SWNT via π- π interactions of the pyrene group whereas the other end is involved in amide bond formation with the ArCuP. Finally, 10 µL of assay composite was drop cast on GCE and dried under a gentle stream of N_2.

iii. Electrocatalysis. Voltammograms were recorded in 80 mM mixed buffer at pH 6.5 with 100 mM KCl. 12.5 mM H_2O_2 (final concentration) and 125 mM substrates (final concentration) were added to the electrochemical cell and the mixture was made homogenous by adding 50 µL of DMSO. The buffer was then saturated with N_2 and LSVs were recorded. For CPE and chronoamperometry experiments, a potential of -950 mV vs Ag/AgCl was applied. After electrolysis, the products were extracted using DCM in a separating funnel and dried over anhydrous Na_2SO_4. The extracted samples was then filtered and injected into GC.

The electrochemical surface coverage of the ArCuPs was determined using eq. (i)

$$i_p = \frac{n^2F^2A\Gamma\nu}{4RT} \qquad \text{(i)}$$

where i_p is the peak current, n is the number of electrons, A is the surface area of the electrode calculated according to a known procedure[21b] from the redox peak shown in Fig. S13, Γ is the surface coverage, ν is the scan rate, and F, R, T represent standard symbols. k_{cat} was determined from eq. (ii)

$$k_{cat} = \frac{j_{cat}}{nF\Gamma} \qquad \text{(ii)}$$

where j_{cat} is the catalytic current density and n is the number of electrons (n = 2 or 4 in this case). k_{uncat} for the uncatalyzed reaction was obtained similarly with the 3SCC-His variant as a control, in the presence of Cu, H_2O_2 and substrates.

Total charge Q passed during electrolysis was used to derive the maximum number of moles of the product from Q/nF. The maximum possible turnover (TON_{max} in Table 2) was calculated from the total charge consumed, where n = 2 or 4 depending on the substrate. K_M for each substrate was determined by chrono-coulometric experiments under varying substrate concentrations (Fig. S1-7).

Hammett analysis. A 1:1 mixture of benzyl alcohol and p-substituted benzyl alcohol at 125 mM were added to an anaerobic solution reaction mixture containing 0.125 mM Cu^I-3SCC, 12.5 mM H_2O_2 at pH 6.5. The reaction was stirred overnight at 37 ºC for 48h and products were extracted in DCM. The log of the ratio of the area under the curve for the p-substituted benzyl alcohol to that of benzyl alcohol was plotted against the σ_p values of the substituents to obtain the Hammett plot.

Gas chromatography. GC experiments were performed in a Shimadzu GC-2014 instrument using a capillary packed column equipped with an auto-sampler liquid injection port. 1 µL of samples were injected and spectra were recorded. The calibration of GC was performed with the respective standard samples to produce calibration curves and quantify products.

ASSOCIATED CONTENT

Supporting Information

The Supporting Information is available free of charge. Detailed electrocatalysis data for all mutants and substrates, pH-dependence, kinetic traces of Cu^{II}-peptides, kcat plot, non-catalytic CVs, CD and thermal melts of the ArCuPs.

AUTHOR INFORMATION

Corresponding Author: *saumenc@olemiss.edu

Notes

The authors declare no competing financial interest.

ACKNOWLEDGEMENTS

S.C. thanks the University of Mississippi for support.

REFERENCES

[1] a) J. Liu, S. Chakraborty, P. Hosseinzadeh, Y. Yu, S. Tian, I. Petrik, A. Bhagi, Y. Lu, *Chem. Rev.* **2014**, *114*, 4366-4469; b) L. M. Mirica, X. Ottenwaelder, T. D. P. Stack, *Chem. Rev.* **2004**, *104*, 1013-1046; c) E. I. Solomon, D. E. Heppner, E. M. Johnston, J. W. Ginsbach, J. Cirera, M. Qayyum, M. T. Kieber-Emmons, C. H. Kjaergaard, R. G. Hadt, L. Tian, *Chem. Rev.* **2014**, *114*, 3659-3853.
[2] G. Vaaje-Kolstad, B. Westereng, S. J. Horn, Z. Liu, H. Zhai, M. Sørlie, V. G. Eijsink, *Science* **2010**, *330*, 219-222.
[3] a) B. Bissaro, Å. K. Røhr, G. Müller, P. Chylenski, M. Skaugen, Z. Forsberg, S. J. Horn, G. Vaaje-Kolstad, V. G. Eijsink, *Nat. Chem. Biol.* **2017**, *13*, 1123; b) B. Bissaro, B. Streit, I. Isaksen, V. G. H. Eijsink, G. T. Beckham, J. L. DuBois, Å. K. Røhr, *Proc. Natl. Acad. Sci., USA* **2020**, *117*, 1504-1513.
[4] a) D. J. Spira-Solomon, E. I. Solomon, *J. Am. Chem. Soc.* **1987**, *109*, 6421-6432; b) D. E. Wilcox, A. G. Porras, Y. T. Hwang, K. Lerch, M. E. Winkler, E. I. Solomon, *J. Am. Chem. Soc.* **1985**, *107*, 4015-4027.
[5] a) L. Bertini, R. Breglia, M. Lambrughi, P. Fantucci, L. De Gioia, M. Borsari, M. Sola, C. A. Bortolotti, M. Bruschi, *Inorg. Chem.* **2018**, *57*, 86-97; b) P. Chylenski, B. Bissaro, M. Sørlie, Å. K. Røhr, A. Várnai, S. J. Horn, V. G. H. Eijsink, *ACS Catal.* **2019**, *9*, 4970-4991; c) S. Kim, J. W. Ginsbach, J. Y. Lee, R. L. Peterson, J. J. Liu, M. A. Siegler, A. A. Sarjeant, E. I. Solomon, K. D. Karlin, *J. Am. Chem. Soc.* **2015**, *137*, 2867-2874; d) S. Kim, C. Saracini, M. A. Siegler, N. Drichko, K. D. Karlin, *Inorg. Chem.* **2012**, *51*, 12603-12605; e) D. Maiti, A. A. Narducci Sarjeant, K. D. Karlin, *Inorg. Chem.* **2008**, *47*, 8736-8747; f) R. L. Peterson, R. A. Himes, H. Kotani, T. Suenobu, L. Tian, M. A. Siegler, E. I. Solomon, S. Fukuzumi, K. D. Karlin, *J. Am. Chem. Soc.* **2011**, *133*, 1702-1705; g) A. Kunishita, M. Kubo, H. Sugimoto, T. Ogura, K. Sato, T. Takui, S. Itoh, *J. Am. Chem. Soc.* **2009**, *131*, 2788-2789; h) S. Paria, T. Ohta, Y. Morimoto, T. Ogura, H. Sugimoto, N. Fujieda, K. Goto, K. Asano, T. Suzuki, S. Itoh, *J. Am. Chem. Soc.* **2015**, *137*, 10870-10873; i) S.-i. Yamazaki, S. Itoh, *J. Am. Chem. Soc.* **2003**, *125*, 13034-13035; j) C. H. Kjaergaard, M. F. Qayyum, S. D. Wong, F. Xu, G. R. Hemsworth, D. J. Walton, N. A. Young, G. J. Davies, P. H. Walton, K. S. Johansen, K. O. Hodgson, B. Hedman, E. I. Solomon, *Proc. Natl. Acad. Sci., USA* **2014**, *111*, 8797.

[6] a) H. J. Davis, T. R. Ward, *ACS Cent. Sci.* **2019**, *5*, 1120-1136; b) F. Schwizer, Y. Okamoto, T. Heinisch, Y. Gu, M. M. Pellizzoni, V. Lebrun, R. Reuter, V. Kohler, J. C. Lewis, T. R. Ward, *Chem. Rev.* **2018**, *118*, 142-231; c) M. Jeschek, R. Reuter, T. Heinisch, C. Trindler, J. Klehr, S. Panke, T. R. Ward, *Nature* **2016**, *537*, 661-665; d) U. Markel, D. F. Sauer, J. Schiffels, J. Okuda, U. Schwaneberg, *Angew. Chem. Int. Ed.* **2019**, *58*, 4454-4464.
[7] S. Mitra, D. Prakash, K. Rajabimoghadam, Z. Wawrzak, P. Prasad, T. Wu, S. K. Misra, J. S. Sharp, I. Garcia-Bosch, S. Chakraborty, *ACS Catal.* **2021**, *11*, 10267-10278.
[8] a) M. Faiella, C. Andreozzi, R. T. M. De Rosales, V. Pavone, O. Maglio, F. Nastri, W. F. DeGrado, A. Lombardi, *Nat. Chem. Biol.* **2009**, *5*, 882-884; b) E. Mathieu, A. E. Tolbert, K. J. Koebke, C. Tard, O. Iranzo, J. E. Penner-Hahn, C. Policar, V. Pecoraro, *Chem. Eur. J.* **2020**, *26*, 249-258; c) A. J. Reig, M. M. Pires, R. A. Snyder, Y. Wu, H. Jo, D. W. Kulp, S. E. Butch, J. R. Calhoun, T. Szyperski, E. I. Solomon, W. F. DeGrado, *Nat. Chem.* **2012**, *4*, 900-906; d) M. Tegoni, F. Yu, M. Bersellini, J. E. Penner-Hahn, V. L. Pecoraro, *Proc. Natl. Acad. Sci., USA* **2012**, *109*, 21234-21239; e) M. L. Zastrow, A. F. A. Peacock, J. A. Stuckey, V. L. Pecoraro, *Nat. Chem.* **2012**, *4*, 118-123.
[9] S. Malayam Parambath, A. E. Williams, L. A. Hunt, D. Selvan, N. I. Hammer, S. Chakraborty, *ChemSusChem* **2021**, *14*, 2237-2246.
[10] a) F. Yu, V. M. Cangelosi, M. L. Zastrow, M. Tegoni, J. S. Plegaria, A. G. Tebo, C. S. Mocny, L. Ruckthong, H. Qayyum, V. L. Pecoraro, *Chem. Rev.* **2014**, *114*, 3495-3578; b) I. V. Korendovych, W. F. DeGrado, *Q. Rev. Biophys.* **2020**, *53*.
[11] a) J. L. Beesley, D. N. Woolfson, *Curr. Opin. Biotechnol.* **2019**, *58*, 175-182; b) D. N. Woolfson, *J. Mol. Biol.* **2021**, 167160; c) J. M. Fletcher, A. L. Boyle, M. Bruning, G. J. Bartlett, T. L. Vincent, N. R. Zaccai, C. T. Armstrong, E. H. C. Bromley, P. J. Booth, R. L. Brady, A. R. Thomson, D. N. Woolfson, *ACS Synth. Biol.* **2012**, *1*, 240-250.
[12] a) M. Mukherjee, A. Dey, *ACS Cent. Sci.* **2019**, *5*, 671-682; b) M. Mukherjee, A. Dey, *Inorg. Chem.* **2020**, *59*, 7415-7425.
[13] a) S. Studer, D. A. Hansen, Z. L. Pianowski, P. R. E. Mittl, A. Debon, S. L. Guffy, B. S. Der, B. Kuhlman, D. Hilvert, *Science* **2018**, *362*, 1285-1288; b) D. Hilvert, *Annu. Rev. Biochem.* **2013**, *82*, 447-470.
[14] M. M. Whittaker, J. W. Whittaker, *Biochemistry* **2001**, *40*, 7140-7148.
[15] B. Bissaro, Å. K. Røhr, M. Skaugen, Z. Forsberg, S. J. Horn, G. Vaaje-Kolstad, V. G. Eijsink, *bioRxiv* **2016**, 097022.
[16] a) J. Hirst, *Biochim. Biophys. Acta* **2006**, *1757*, 225-239; b) A. P. Brown, F. C. Anson, *Anal. Chem.* **1977**, *49*, 1589-1595.
[17] N. M. Marshall, D. K. Garner, T. D. Wilson, Y.-G. Gao, H. Robinson, M. J. Nilges, Y. Lu, *Nature* **2009**, *462*, 113-116.
[18] a) F. L. Aachmann, M. Sørlie, G. Skjåk-Bræk, V. G. Eijsink, G. Vaaje-Kolstad, *Proc. Natl. Acad. Sci.* **2012**, *109*, 18779-18784; b) S. Chauhan, P. Hosseinzadeh, Y. Lu, N. J. Blackburn, *Biochemistry* **2016**, *55*, 2008-2021; c) F. Jacobson, A. Pistorius, D. Farkas, W. De Grip, Ö. Hansson, L. Sjölin, R. Neutze, *J. Biol. Chem.* **2007**, *282*, 6347-6355; d) S. Suzuki, K. Yamaguchi, K. Kataoka, K. Kobayashi, S. Tagawa, T. Kohzuma, S. Shidara, H. Iwasaki, *J. Biol. Inorg. Chem.* **1997**, *2*, 265-274.
[19] a) J. Walshaw, D. N. Woolfson, *Biochem. Soc. Trans.* **2000**, *28*, A423-A423; b) C. I. Branden, J. Tooze, *Introduction to protein structure*, Garland Science, **2012**.
[20] G. Roelfes, *Acc. Chem. Res.* **2019**, *52*, 545-556.
[21] a) S. Chakraborty, S. Babanova, R. C. Rocha, A. Desireddy, K. Artyushkova, A. E. Boncella, P. Atanassov, J. S. Martinez, *J. Am. Chem. Soc.* **2015**, *137*, 11678-11687; b) Z. Nazemi, P. Prasad, S. Chakraborty, *ChemElectroChem* **2020**, *7*, 1029-1037.